ACS APPLIED ELECTRONIC MATERIALS

Open Access
This article is licensed under CC-BY-NC-ND 4.0

pubs.acs.org/acsaelm
Article

High Performance of an In-Material Reservoir Computing Device Achieved by Complex Dynamics in a Nanoparticle Random Network Memristor

Oradee Srikimkaew, Deep Banerjee, Saman Azhari, Yuki Usami, and Hirofumi Tanaka*

Cite This: ACS Appl. Electron. Mater. 2024, 6, 688–695
Read Online

ACCESS | Metrics & More | Article Recommendations | Supporting Information

ABSTRACT: An in-material reservoir computing (RC) device with an Ag–Ag_2S core–shell nanoparticle (NP) network is proposed. Network-wide nonlinear sine-wave outputs of higher frequencies and varying phases were produced from the different Ag^+ ion diffusion rates and filament formation caused by the heterogeneous NP size in the thiol layer. Such emergent dynamics of multiple information regimes enabled the reconstruction of Fourier waves, with a maximum accuracy of 99% achieved only for trained outputs with mixed spatiotemporal complexities. Additionally, the device showed stable retrieval of past information with a two-times-step delay and successfully computed a two-step time-series prediction task with 87% accuracy.

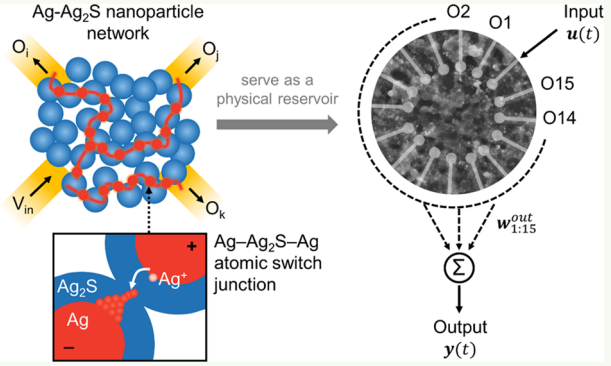

KEYWORDS: *silver–silver sulfide nanoparticle, atomic switch network, volatile resistive switching, material intelligence, neuromorphic AI hardware, physical reservoir*

INTRODUCTION

Reservoir computing (RC) is a computing paradigm in which artificial neural networks are used to process time-dependent inputs efficiently.[1] This approach was originally developed as an altered version of a recurrent neural network (RNN).[2,3] In an RC system, the input and internal weights of a network are kept fixed, and only the connection weights (readout) between the reservoir and output are trained using a simple learning algorithm, such as linear regression. Consequently, the computational cost of training an RC system can be minimized compared to that of a conventional RNN.[1] RC can reduce power consumption and has therefore recently attracted increasing interest in hardware implementations as a way to avoid the von Neumann bottleneck.[4,5] In RC systems, the reservoir serves to nonlinearly transform time-dependent inputs into extractable high-feature outputs; therefore, many physical systems (compared with their software counterparts) with intrinsic nonlinear dynamics have been used as in-material reservoirs. Materials such as ferromagnets,[6−8] ferroelectrics,[9,10] doped inorganic polyoxometalate,[11] carbon nanotube/polyoxometalate networks,[12,13] metal-oxide memristors,[14−16] atomic switch networks (ASNs),[17−19] and conductive polymer networks[20] have been proposed for realizing a physical reservoir. A physical reservoir with ASNs is considered the most promising platform for implementing hardware-based RC; in such a platform, the emergent dynamics are generated by the whole network system rather than by tuning individual elements.[17] For realizing such a platform, typically, a self-assembled metallic nanowire network is coated with memristive materials like Ag_2S,[21] TiO_2,[22] or poly(vinylpyrrolidone).[18] As a result, each network junction acts as an atomic switch that, like a biological synapse, processes spatiotemporal input data nonlinearly via electrochemical interaction to realize biologically plausible in-memory parallel computing.

Our research group has previously used an ASN with Ag–Ag_2S core–shell nanoparticles (NPs) to realize a physical reservoir in which nonlinear dynamics arise via the movement of Ag ions between the Ag/Ag_2S/Ag junction of two NPs.[19] The NP network reservoir was used to perform classification tasks that generate signals of different frequencies or shapes. However, the effect of nonlinear complexity via Ag ion migration on RC performance has not been investigated in detail. In this study, we investigate the nonlinear forms of the NP network reservoir and the influence of multiple nonlinearities on the RC performance. We experimentally demonstrated a physical RC system by using Ag–Ag_2S NP

Received: August 3, 2023
Revised: November 29, 2023
Accepted: November 30, 2023
Published: December 26, 2023

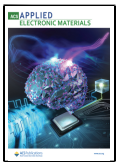

Downloaded via KYUSHU INST OF TECHNOLOGY on July 22, 2024 at 05:14:08 (UTC).
See https://pubs.acs.org/sharingguidelines for options on how to legitimately share published articles.

© 2023 The Authors. Published by American Chemical Society

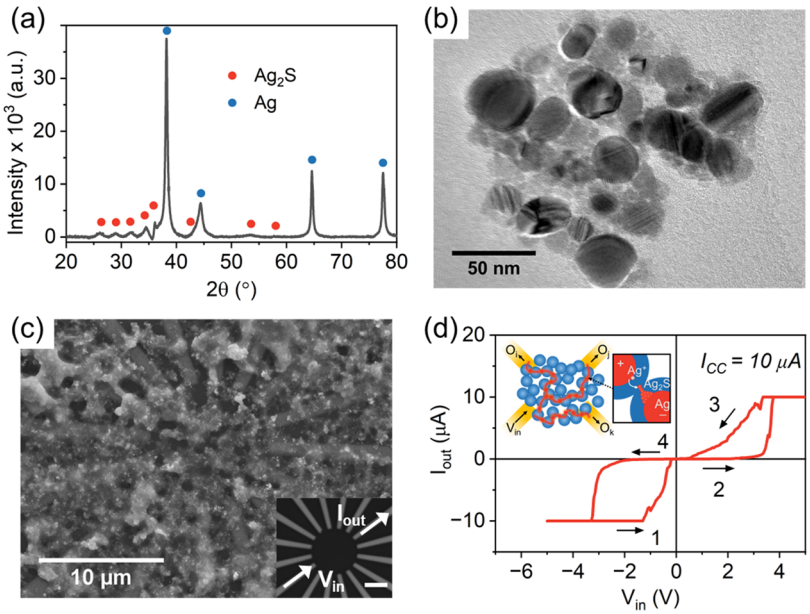

Figure 1. (a) XRD pattern and (b) TEM image of Ag−Ag_2S NPs. (c) SEM image of the Pt/Ag−Ag_2S NPs/Pt device. The inset shows an optical image of 16-terminal electrodes with a 5 μm scale bar. (d) $I-V$ characteristics were measured in the electrode pair indicated in inset (c). The inset shows an illustration of conductive pathways forming through the Ag/Ag_2S/Ag junction due to the redox reaction.

network-based 16-terminal devices. This device is operated as a memristor and exhibits volatile resistive switching. In our RC system, the outputs at different terminals were collected simultaneously to investigate the complexity of the simultaneous dynamical responses. The benchmark tasks for RC, such as waveform generation, short-term memory capacity (MC), and second-order nonlinear autoregressive moving average (NARMA2) tasks, were tested and verified. Different nonlinear shapes were analyzed, and the results show that output signals with intricate or multiple nonlinear forms yield a greater testing accuracy. The significant increase in accuracy highlights the potential of volatile Ag−Ag_2S NP network-type memristors in physical RC.

EXPERIMENTAL SECTION

Ag−Ag_2S NPs were synthesized at 25 °C via the modified Brust-Schiffrin procedure[23,24] with Ag: thiol molar ratios of 0.25:1. Briefly, a mixture of allylmercaptan (AM, 0.94% v/v in toluene), silver nitrate (1% w/v in water), tetraoctylammonium bromide (0.93% w/v in toluene), and sodium borohydride (1.8% w/v in water) was stirred vigorously at 25 °C until the mixture changed from yellow to brown. After removing the aqueous phase, the remaining brown solution was diluted with ethanol (400 mL), refrigerated (4 h), and washed five times with ethanol again to remove the residual organic AM by centrifugation. The obtained NPs were then resuspended in ethanol by sonication and subsequently used to produce the in-material RC device. The device was initially patterned with a Ti/Pt (6:24 nm) 16-electrode array on a SiO_2/Si (500 nm thickness) substrate by optical lithography, following which the NPs suspension was drop-casted on the central electrode pads and dried at 100 °C for 5 min. Transmission electron microscopy (TEM) and scanning electron microscopy (SEM) were performed using JEOL JEM-2100Plus and JEOL JSM-7800F, respectively. X-ray diffraction spectroscopy (XRD) was performed using a Rigaku Smart Lab with a Cu−Kα source. $I-V$ measurements were performed by using a semiconductor parameter analyzer (Agilent 4156 B).

In order to perform the RC tasks, a data acquisition system (National Instruments PXIe-6363 and SCB-68A) and a custom LabVIEW program were used to apply the input signals and record the output responses (Figures S1 and 2a). An analogue output from the PXIe-6363 (output impedance, Z_{out} = 0.2 Ω) was applied to the in-material RC device, which functioned as an input signal. The input signal constituted an 11 Hz sine wave with an amplitude of ±4 V for the waveform generation task, ±4 V random white noise for the NARMA2 task, and ±4 V Boolean-like pulse sequence for the short-term MC task. The output signals from the device were collected through the SCB-68A multiterminal connector with load resistors (R_L = 2.7 MΩ) and then transmitted to the PXIe-6363 as input signals (input impedance, Z_{in} > 10 GΩ; input capacitance, C_{in} = 100 pF). A total of 15 outputs were collected simultaneously over 60 s, with a sampling rate of 1000 point/s. A total epoch of 1 s was used for training and testing. Fast Fourier transformation (FFT) was performed using Origin Pro software. Waveform generation, MC, and NARMA2 were executed by using Python software. Electrochemical impedance spectroscopy (EIS) was conducted by using a PC-based oscilloscope with an impedance analyzer (Digilent Analog Discovery 2, 410−321). The EIS measurements were performed using an ±50 mV AC amplitude with varying frequencies from 100 mHz to 1 MHz and a DC bias of 0 V with a resistance value of 10 kΩ.

RESULTS AND DISCUSSION

The morphology of Ag−Ag_2S NPs was investigated using XRD and TEM. The XRD pattern in Figure 1a shows two phases of monoclinic Ag_2S and metallic Ag. A comprehensive analysis of the NP structure has been performed in ref 23 the NPs are composed of an Ag core surrounded by Ag_2S, making the junction between two particles an atomic switch.[24] The TEM image (Figure 1b) shows NPs with nearly spherical shapes and diameters of 38 ± 16 nm. The radius of the Ag core layer and the Ag_2S shell thickness were 18 ± 8 and 1.0 ± 0.4 nm, respectively (see Supporting Information). As shown in Figure 1c, the SEM image of the Pt/Ag−Ag_2S NPs/Pt devices reveals the aggregated NPs and the networked distribution of NPs. Assuming a two-dimensional network, our NP network reservoir consists of ~10^5 random synaptic switch junctions in the central region (78.5 μm^2) between radial electrodes (⌀ = 10 μm), making it analogous to a dense biological neural network.[25] The nonlinear behavior of the device was investigated by applying a voltage sweep. Figure 1d shows

https://doi.org/10.1021/acsaelm.3c01046
ACS Appl. Electron. Mater. 2024, 6, 688−695

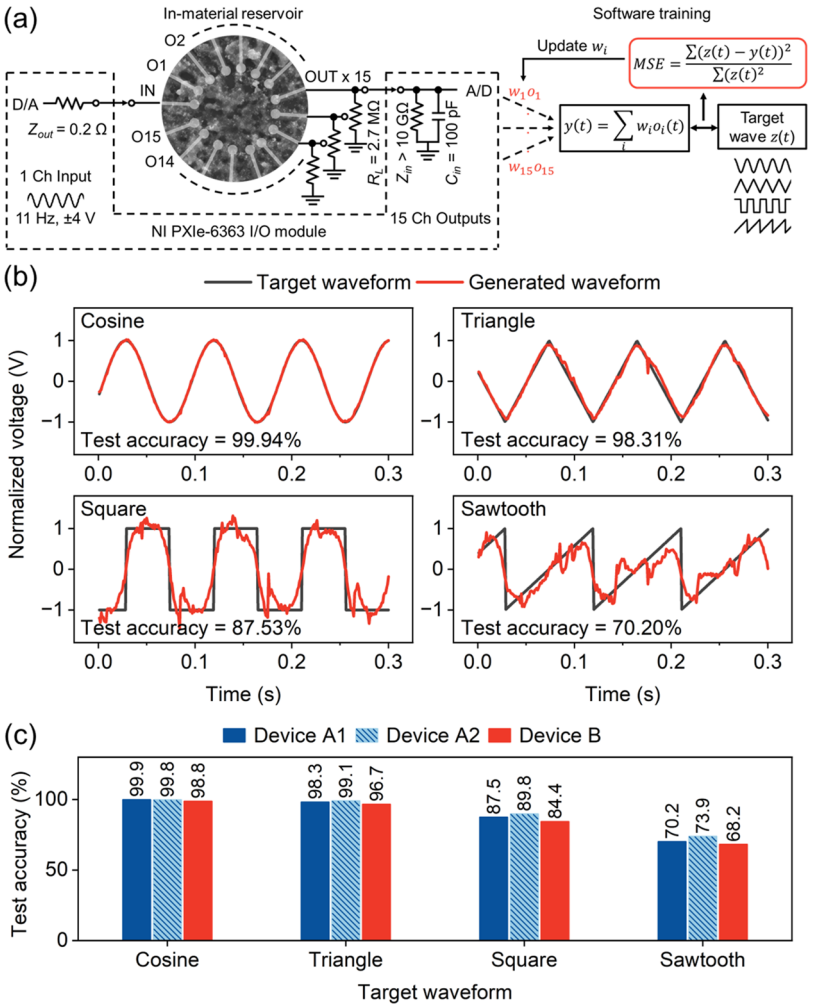

Figure 2. (a) Schematics of physical RC system implemented on the Pt/Ag−Ag_2S NPs/Pt device. (b) Testing performance of the waveform generation task performed using 15 output readouts of Device A1. (c) Variation of test accuracy performed on Device A after one year of storage, indicated by Device A2, and on a different device, identified as Device B.

the $I-V$ characteristics of the device obtained from the electrodes indicated in the inset of Figure 1c with a compliance current (I_{CC}) of 10 μA. The $I-V$ curve shows volatile switching with both positive and negative bias. As the voltage increased (indicated as 2 and 4), the device remained in the high-resistance state (HRS) and subsequently switched to the low-resistance state (LRS) at a voltage of approximately ±3.5 V. When the voltage was removed (indicated as 1 and 3), the current spontaneously returned to its initial state of HRS before reaching zero bias, resulting in volatile resistive switching behavior.[26,27] This switching behavior of the Ag−Ag_2S NP-based ASN can be attributed to conductive pathways between the electrodes. When a voltage bias (Vin) is applied to the input electrode with respect to the output electrode (O), the pathway with the lowest resistance is selected as the conductive path of those electrode pairs, as illustrated in the inset of Figure 1d. The conductive pathways are formed through the formation of Ag filaments at the Ag/Ag_2S/Ag junctions owing to electrochemical reactions.[17,28−30] This creates a network of conductive junctions that link the NPs, leading to the formation of a unique conductive pathway between the electrodes. The connections persist for varying durations depending on the programming voltage or established conductive pathway,[31,32] thus generating the temporal component and complexity of the network. The $I-V$ characteristics of the device were examined by conducting multiple sweeping cycles and varying the I_{CC} levels, as shown in Figure S3. The switching behavior remained volatile, while the shape and switching voltage exhibited variation across sweeping cycles. The variation indicates a variety of nonlinear dynamics, which is suitable for constructing physical RC systems.

A primitive feature of RC is the ability to classify the low-dimensional states of an input and map the signals into higher-dimensional states by generating signals of different frequencies or shapes.[21] The higher-dimensional mapping ability of the device was investigated by performing a waveform generation task, in which a sine wave was reconstructed into various specific waveforms. We constructed the physical RC system by using the nonlinearity of the device that results from its memristive behavior, as shown schematically in Figure 2a. A sine wave input (V_{in}; ± 4 V, 11 Hz) was applied to the NP network reservoir, and 15 output responses (O1−O15) were collected simultaneously. The output signals were linearly combined, and the output weights (w_i) were trained offline by comparing the output with the target waveforms: cosine, triangle, square, and sawtooth. A waveform was then reconstructed using trained weights. To test the goodness of

https://doi.org/10.1021/acsaelm.3c01046
ACS Appl. Electron. Mater. 2024, 6, 688−695

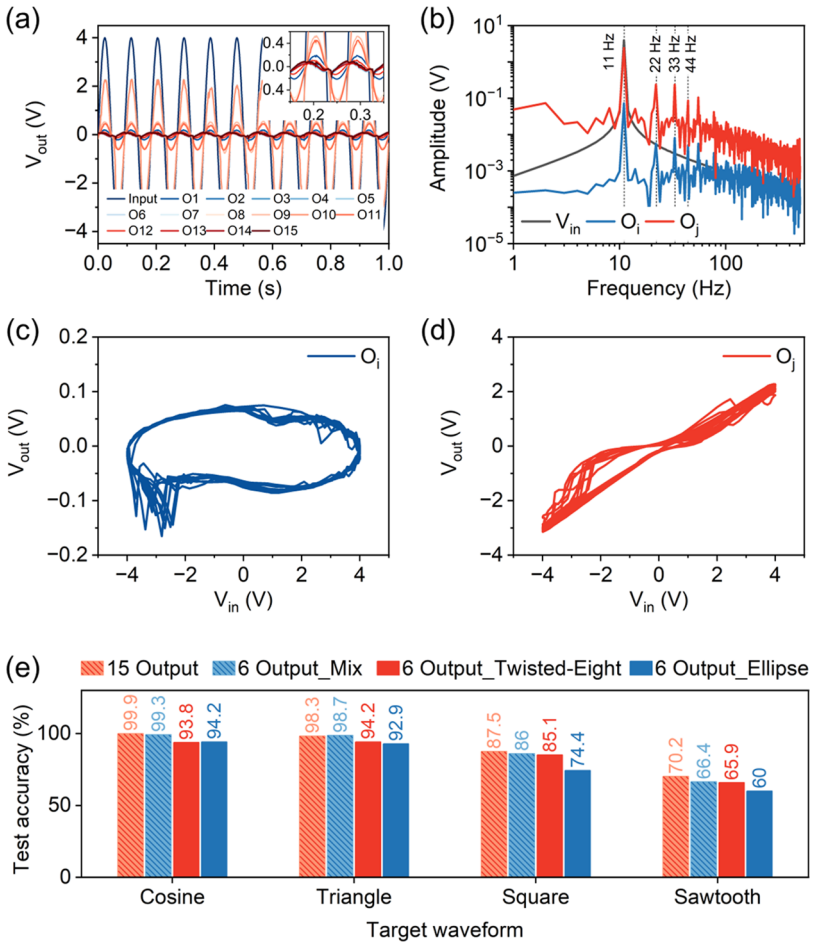

Figure 3. (a) 15 output responses were obtained simultaneously. (b) FFT results indicate higher harmonics of the input frequency 22 Hz, 33 Hz, 44 Hz, etc. The index "*i*" indicates electrode pad numbers 2−6 and 12−15, and the index "*j*" indicates pad numbers 1 and 7−11. The LP of the output responses exhibited multiple nonlinear forms with a distorted ellipse (c) and a twisted-eight (d). (e) Variation of test accuracy performed with different numbers of tested outputs (15 and six) and different nonlinearity forms (ellipse, twisted-eight, and mixed). Six outputs were used for the ellipse and twisted-eight cases, and three outputs of both the ellipse and twisted-eight forms were used for the mixed case.

the model, the performance was evaluated by calculating the normalized mean squared error (NMSE) using eq 1 between the target $z(t)$ and the output $y(t)$, where accuracy is defined as the difference between NMSE and unity.[12]

$$\mathrm{NMSE} = \frac{\sum (z(t) - y(t))^2}{\sum (z(t)^2} \tag{1}$$

Figure 2b shows the test accuracy of the generated waveforms constructed using 15 outputs. The cosine and triangle waveforms show a negligible mismatch between the target and generated waveforms, with the accuracy being ∼99%. By contrast, the generated square and sawtooth waveforms show a significant mismatch with the target, leading to a decrease in accuracy. Figure 2c shows the variation of a waveform generation task examined under two conditions: (1) using the same device after one year of storage (Device A1 and A2), and (2) using a different device (Device B). The mean accuracy values of each waveform were highly consistent, resulting in an insignificant variance. Compared to a previous study using a single crossbar memristor,[33] the operating power of our Ag−Ag_2S NP memristor-based RC system exhibited a significant reduction (Supporting Information), which makes it appropriate for future high-density device applications.

To clarify the higher-dimensional mapping ability, we further investigated the output responses, as shown in Figure 3a. It is worth noting that the output values are the apparent values with respect to the load resistance (Figure 2a). The output signals exhibited a variation in their similarity of amplitudes and phases compared to the input, indicating the ability to produce a diverse class of dynamical output responses.[34] The outputs were also converted in a frequency domain by using FFT, as shown in Figure 3b. The frequency profiles show that the output signals contain a higher harmonic of the input frequency, thus enabling the generation of signals of different frequencies or shapes. Such higher harmonic generation is a common phenomenon observed in various nonlinear systems based on physical reservoirs.[9,12,20,35] The variation of output responses were again investigated based on the Lissajous plot (LP), where the output was plotted against the input signal (V_{in} vs V_{out}).[36] Interestingly, the LP profiles can be separated into two distinct nonlinear forms, as shown in Figure 3c,d. Figure 3c shows a distorted ellipse with a large phase shift and attenuated amplitude. By contrast, Figure 3d shows the shape of a twisted-eight with an in-phase LP and a slight decrease in amplitude. The impedance analysis was conducted to understand the underlying cause of such distinct nonlinear forms. The Nyquist plot of electrodes with a distorted ellipse shape

https://doi.org/10.1021/acsaelm.3c01046
ACS Appl. Electron. Mater. 2024, 6, 688−695

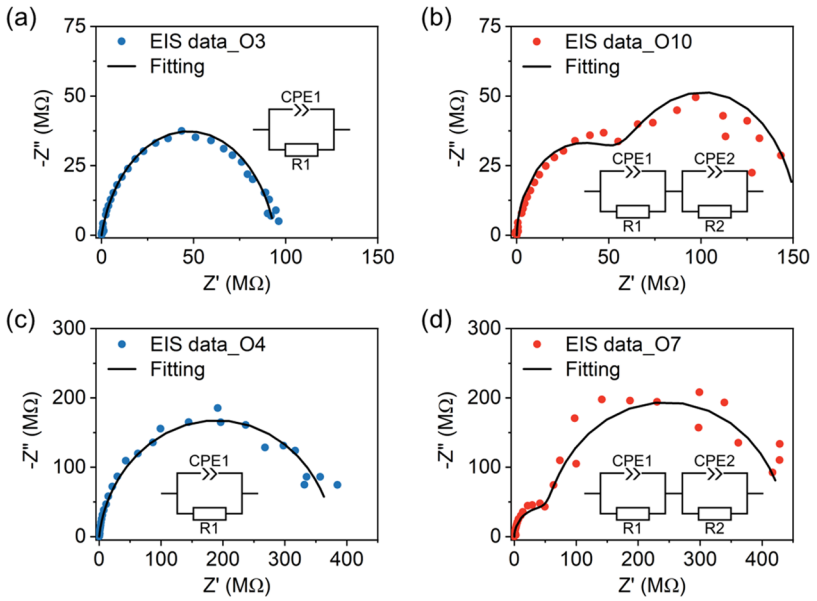

Figure 4. Nyquist plot of electrodes correlated with a distorted ellipse shape (a, c), and a twisted-eight shape (b, d). Insets display the correlated equivalent circuits, where R is a resistor and CPE is a constant phase element that represents a nonideal capacitor.

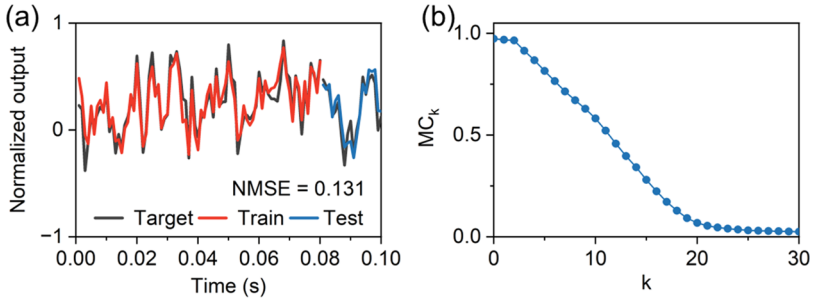

Figure 5. Time-series data prediction and echo-state property, demonstrated by our physical RC system. (a) Training and testing performance of NARMA2 task. (b) Correlation between the target and the predicted signals MC_k and time-step delay k.

exhibited a well-defined semicircular arc, as shown in Figure 4a,c. The equivalent circuits in the inset demonstrated a resistance−capacitance (RC) circuit component corresponding to the NP-electrode interface. Conversely, the Nyquist plot of electrodes correlated with a twisted-eight shape exhibited two semicircular arcs (Figure 4b,d), and their equivalent circuits show the existence of two RC circuits. The second semicircle can be attributed to mass transfer phenomena owing to the formation of filaments or the behavior of the electrical double layer at the interface of the Ag−Ag_2S NP network. This behavior is a consequence of the established Ag filament and is consistent with findings from a previous study.[37] The presence of different nonlinear forms further highlights the NP reservoir's ability to produce multiple dynamics and nonlinearity.[38]

To verify the effect of complex nonlinearity on the reservoir performance, we performed waveform generation by using six outputs with different forms of nonlinearity: ellipse, twisted-eight, and mixed. The test performances of all waveforms are shown in Figure 3e. The twisted-eight form surpasses the ellipse in terms of accuracy with triangle, square, and sawtooth waveforms because of the lower levels of odd harmonics in the output (as shown in Figure 3b), which can interfere with the replication of a triangular waveform. However, the twisted-eight form does contain higher harmonics with varying amplitudes (Figure 3a), resulting in improved accuracy for square and sawtooth waveforms. A cosine waveform requires phase-shifted sine wave outputs; therefore, the ellipse showed greater accuracy than the twisted-eight. In the mixed form, the output signals contained multiple forms of nonlinearity with various amplitudes, phases, and frequencies; this resulted in the highest testing accuracy.[12] Moreover, the testing accuracy of the mixed case showed a slight decrease when compared to the 15 signals case. Prior studies have shown that higher accuracy can be achieved by increasing the number of outputs.[19] The above analysis thus emphasizes the fact that output signals with more complex or multiple nonlinear responses also offer higher testing accuracy.

Owing to the typical application of the reservoir system in spatiotemporal information processing, the ability of the NP network reservoir to analyze time-series data and tackle nonlinear dynamic problems was also investigated. In keeping with the methodology of a previous study,[39,40] we conducted a NARMA2 task. Our RC system was trained using a random white noise signal with voltage fluctuation. A total epoch of 1 s was used for training and testing with a training ratio of 0.8. The output signals were linearly combined and trained with a ridge regression training algorithm. The target signal was constructed by the following equation:

https://doi.org/10.1021/acsaelm.3c01046
ACS Appl. Electron. Mater. 2024, 6, 688−695

$$y(t) = 0.4y(t-1) + 0.4y(t-1)y(t-2) + 0.6u^3(t) + 0.1 \quad (2)$$

where $y(t)$ and $u(t)$ are the given input and output at time frame t, respectively. Figure 5a shows the training and testing performances of the NARMA2 task. After training, the reconstructed output (blue line) closely followed the target signal (gray line) with a calculated NMSE of 0.131; this is almost the same value as that of other systems using a physical RC-based random network.[40,41] To interpret this ability, we performed a short-term MC task that can be determined by calculating the number of precise recalls of an input signal delayed by a time step (k).[20,40] In this task, the input signal was randomly generated as a Boolean-like pulse sequence in which the positive (negative) pulse (4/−4 V) was used to indicate "1" ("0"). MC_k represents the correlation between the target and output signals and is expressed as follows

$$MC_k = \frac{\mathrm{cov}^2[p_{\mathrm{train}}(k), p_{\mathrm{out}}(k)]}{\mathrm{var}[p_{\mathrm{train}}(k)]\mathrm{var}[p_{\mathrm{out}}(k)]} \quad (3)$$

$$MC = \sum_{k=1}^{k_{\max}} MC_k \quad (4)$$

where cov, var., p_{train}, and p_{out} are the covariance, variance, training pulse, and output pulse, respectively. Figure 5b shows that MC_k remains high until $k = 2$, following which it gradually decreases with the calculated MC of 12.15. This suggests that the NP network reservoir can accurately reconstruct the signal for an input delayed by up to two timesteps. Therefore, our RC system has a low prediction error for the NARMA2 task.[40]

CONCLUSIONS

In summary, we demonstrated that the form of nonlinearity strongly impacts the performance of an RC system based on the Ag−Ag_2S NPs network device. Our results indicate that the presence of multiple nonlinear forms in the output signals can significantly enhance the accuracy of the RC waveform generation task. The LP profiles showed various nonlinearities that arise from the memristive behavior throughout the ASNs. Furthermore, benchmark RC tasks for time-series data prediction (NARMA2) and MC were also performed, and the calculated prediction error was 0.131. The volatile switching behavior permits the device to store information for a short-term period, thus allowing it to learn the input signal and potentially solve a second-order nonlinear problem. This study primarily explains the importance of utilizing an NP network reservoir with the capability of generating diverse nonlinear dynamics in a physical RC system. In the future, this device will be integrated with an electrical circuit to implement the in-material RC and potentially enhance the efficiency of the computing system.

ASSOCIATED CONTENT

Supporting Information

The Supporting Information is available free of charge at https://pubs.acs.org/doi/10.1021/acsaelm.3c01046.

Additional data acquisition details, core−shell thickness calculation, and estimated power consumption (PDF)

AUTHOR INFORMATION

Corresponding Author

Hirofumi Tanaka − *Graduate School of Life Science and Systems Engineering, Kyushu Institute of Technology (Kyutech), Kitakyushu 808-0196, Japan; Research Center for Neuromorphic AI Hardware, Kyutech, Kitakyushu 808-0196, Japan; Institute of Science, Suranaree University of Technology, Nakhon Ratchasima 30000, Thailand;* orcid.org/0000-0002-4378-5747; Email: tanaka@brain.kyutech.ac.jp

Authors

Oradee Srikimkaew − *Graduate School of Life Science and Systems Engineering, Kyushu Institute of Technology (Kyutech), Kitakyushu 808-0196, Japan;* orcid.org/0000-0002-3990-8513

Deep Banerjee − *Graduate School of Life Science and Systems Engineering, Kyushu Institute of Technology (Kyutech), Kitakyushu 808-0196, Japan; Research Center for Neuromorphic AI Hardware, Kyutech, Kitakyushu 808-0196, Japan;* orcid.org/0000-0003-1726-1867

Saman Azhari − *Graduate School of Life Science and Systems Engineering, Kyushu Institute of Technology (Kyutech), Kitakyushu 808-0196, Japan; Research Center for Neuromorphic AI Hardware, Kyutech, Kitakyushu 808-0196, Japan;* Present Address: Graduate School of Information, Production and Systems, Waseda University, 2−7 Hibikino, Wakamatsu, Kitakyushu, Fukuoka 808−0135, Japan; orcid.org/0000-0002-7043-0909

Yuki Usami − *Graduate School of Life Science and Systems Engineering, Kyushu Institute of Technology (Kyutech), Kitakyushu 808-0196, Japan; Research Center for Neuromorphic AI Hardware, Kyutech, Kitakyushu 808-0196, Japan;* orcid.org/0000-0002-8583-325X

Complete contact information is available at: https://pubs.acs.org/10.1021/acsaelm.3c01046

Notes

The authors declare no competing financial interest.

ACKNOWLEDGMENTS

The authors would like to thank Profs. T. Morie and K. Tateno of Kyutech for the fruitful discussions. This work was technologically supported by Yamaguchi University and Kitakyushu Semiconductor Center under the "Advanced Research Infrastructure for Materials and Nanotechnology in Japan (ARIM Japan)" of the Ministry of Education, Culture, Sports, Science and Technology (MEXT), Japan. This work was financially supported by KAKENHI (grant nos. 19H02559, 19K22114, 20K21819, 21K14527, 22H01900, 23K17864 and 23K18495), JST CREST (grant no. JPMJCR21B5), ACT-X (grant no. JPMJAX22K4), ALCA-Next (Grant No. JPMJAN23F3), and JSPS Core-to-Core Program (JPJSCCA20220006). Y.U. and S.A. thank Asahi Kohsan Co., Ltd. for financial support through the Kitakyushu Foundation for the Advancement of Industry, Science, and Technology, Japan. H.T. also thanks to support from Thailand Science Research and Innovation (TSRI) and National Science, Research and Innovation Fund (NSRF), Thailand (NRIIS Project Number 90465).

https://doi.org/10.1021/acsaelm.3c01046
ACS Appl. Electron. Mater. 2024, 6, 688−695

REFERENCES

(1) Lukoševičius, M.; Jaeger, H. Reservoir Computing Approaches to Recurrent Neural Network Training. *Comput. Sci. Rev.* **2009**, *3* (3), 127−149.

(2) Jaeger, H.; Haas, H. Harnessing Nonlinearity: Predicting Chaotic Systems and Saving Energy in Wireless Communication. *Science* **2004**, *304* (5667), 78−80.

(3) Verstraeten, D.; Schrauwen, B.; D'Haene, M.; Stroobandt, D. An Experimental Unification of Reservoir Computing Methods. *Neural Networks* **2007**, *20* (3), 391−403.

(4) Tanaka, G.; Yamane, T.; Héroux, J. B.; Nakane, R.; Kanazawa, N.; Takeda, S.; Numata, H.; Nakano, D.; Hirose, A. Recent Advances in Physical Reservoir Computing: A Review. *Neural Networks* **2019**, *115*, 100−123.

(5) Nakajima, K. Physical Reservoir Computing-an Introductory Perspective. *Jpn. J. Appl. Phys.* **2020**, *59* (6), No. 060501.

(6) Akashi, N.; Kuniyoshi, Y.; Tsunegi, S.; Taniguchi, T.; Nishida, M.; Sakurai, R.; Wakao, Y.; Kawashima, K.; Nakajima, K. A Coupled Spintronics Neuromorphic Approach for High-Performance Reservoir Computing. *Adv. Intell. Syst.* **2022**, *4* (10), No. 2200123.

(7) Nakane, R.; Tanaka, G.; Hirose, A. Reservoir Computing with Spin Waves Excited in a Garnet Film. *IEEE Access* **2018**, *6*, 4462−4469.

(8) Jiang, W.; Chen, L.; Zhou, K.; Li, L.; Fu, Q.; Du, Y.; Liu, R. H. Physical Reservoir Computing Using Magnetic Skyrmion Memristor and Spin Torque Nano-Oscillator. *Appl. Phys. Lett.* **2019**, *115* (19), No. 192403.

(9) Liu, K.; Dang, B.; Zhang, T.; Yang, Z.; Bao, L.; Xu, L.; Cheng, C.; Huang, R.; Yang, Y. Multilayer Reservoir Computing Based on Ferroelectric α-In2Se3 for Hierarchical Information Processing. *Adv. Mater.* **2022**, *34* (48), No. 2108826.

(10) Chen, Z.; Li, W.; Fan, Z.; Dong, S.; Chen, Y.; Qin, M.; Zeng, M.; Lu, X.; Zhou, G.; Gao, X.; Liu, J. M. All-Ferroelectric Implementation of Reservoir Computing. *Nat. Commun.* **2023**, *14* (1), No. 3585.

(11) Zhang, G.; Xiong, Z. Y.; Gong, Y.; Zhu, Z.; Lv, Z.; Wang, Y.; Yang, J. Q.; Xing, X.; Wang, Z. P.; Qin, J.; Zhou, Y.; Han, S. T. Polyoxometalate Accelerated Cationic Migration for Reservoir Computing. *Adv. Funct. Mater.* **2022**, *32* (45), No. 2204721.

(12) Banerjee, D.; Kotooka, T.; Azhari, S.; Usami, Y.; Ogawa, T.; Gimzewski, J. K.; Tamukoh, H.; Tanaka, H. Emergence of In-Materio Intelligence from an Incidental Structure of a Single-Walled Carbon Nanotube−Porphyrin Polyoxometalate Random Network. *Adv. Intell. Syst.* **2022**, *4* (4), No. 2100145.

(13) Tanaka, H.; Akai-Kasaya, M.; Termehyousefi, A.; Hong, L.; Fu, L.; Tamukoh, H.; Tanaka, D.; Asai, T.; Ogawa, T. A Molecular Neuromorphic Network Device Consisting of Single-Walled Carbon Nanotubes Complexed with Polyoxometalate. *Nat. Commun.* **2018**, *9* (1), No. 2693.

(14) Midya, R.; Wang, Z.; Asapu, S.; Zhang, X.; Rao, M.; Song, W.; Zhuo, Y.; Upadhyay, N.; Xia, Q.; Yang, J. J. Reservoir Computing Using Diffusive Memristors. *Adv. Intell. Syst.* **2019**, *1* (7), No. 1900084.

(15) Wang, S.; Li, Y.; Wang, D.; Zhang, W.; Chen, X.; Dong, D.; Wang, S.; Zhang, X.; Lin, P.; Gallicchio, C.; Xu, X.; Liu, Q.; Cheng, K. T.; Wang, Z.; Shang, D.; Liu, M. Echo State Graph Neural Networks with Analogue Random Resistive Memory Arrays. *Nat. Mach. Intell.* **2023**, *5* (2), 104−113.

(16) Moon, J.; Ma, W.; Shin, J. H.; Cai, F.; Du, C.; Lee, S. H.; Lu, W. D. Temporal Data Classification and Forecasting Using a Memristor-Based Reservoir Computing System. *Nat. Electron.* **2019**, *2* (10), 480−487.

(17) Sillin, H. O.; Aguilera, R.; Shieh, H.-H.; Avizienis, A. V.; Aono, M.; Stieg, A. Z.; Gimzewski, J. K. A Theoretical and Experimental Study of Neuromorphic Atomic Switch Networks for Reservoir Computing. *Nanotechnology* **2013**, *24* (38), No. 384004.

(18) Milano, G.; Pedretti, G.; Montano, K.; Ricci, S.; Hashemkhani, S.; Boarino, L.; Ielmini, D.; Ricciardi, C. In Materia Reservoir Computing with a Fully Memristive Architecture Based on Self-Organizing Nanowire Networks. *Nat. Mater.* **2022**, *21* (2), 195−202.

(19) Hadiyawarman; Usami, Y.; Kotooka, T.; Azhari, S.; Eguchi, M.; Tanaka, H. Performance of Ag−Ag2S Core−Shell Nanoparticle-Based Random Network Reservoir Computing Device. *Jpn. J. Appl. Phys.* **2021**, *60* (SC), No. SCCF02.

(20) Usami, Y.; van de Ven, B.; Mathew, D. G.; Chen, T.; Kotooka, T.; Kawashima, Y.; Tanaka, Y.; Otsuka, Y.; Ohoyama, H.; Tamukoh, H.; Tanaka, H.; van der Wiel, W. G.; Matsumoto, T. In-Materio Reservoir Computing in a Sulfonated Polyaniline Network. *Adv. Mater.* **2021**, *33* (48), No. 2102688.

(21) Demis, E. C.; Aguilera, R.; Scharnhorst, K.; Aono, M.; Stieg, A. Z.; Gimzewski, J. K. Nanoarchitectonic Atomic Switch Networks for Unconventional Computing. *Jpn. J. Appl. Phys.* **2016**, *55* (11), No. 1102B2.

(22) Li, Q.; Diaz-Alvarez, A.; Tang, D.; Higuchi, R.; Shingaya, Y.; Nakayama, T. Sleep-Dependent Memory Consolidation in a Neuromorphic Nanowire Network. *ACS Appl. Mater. Interfaces* **2020**, *12* (45), 50573−50580.

(23) Battocchio, C.; Meneghini, C.; Fratoddi, I.; Venditti, I.; Russo, M. V.; Aquilanti, G.; Maurizio, C.; Bondino, F.; Matassa, R.; Rossi, M.; Mobilio, S.; Polzonetti, G. Silver Nanoparticles Stabilized with Thiols: A Close Look at the Local Chemistry and Chemical Structure. *J. Phys. Chem. C* **2012**, *116* (36), 19571−19578.

(24) Hadiyawarman; Eguchi, M.; Tanaka, H. Control of the Neuromorphic Learning Behavior Based on the Aggregation of Thiol-Protected Ag-Ag_2S Core-Shell Nanoparticles. *Jpn. J. Appl. Phys.* **2020**, *59* (1), No. 015001.

(25) Kandel, E. R.; Schwartz, J. H.; Jessell, T. M.; Siegelbaum, S. A.; Hudspeth, A. J. *Principles of Neural Science*, 5th ed.; McGraw Hill: New York, 2014.

(26) Wang, Z.; Joshi, S.; Savel'ev, S. E.; Jiang, H.; Midya, R.; Lin, P.; Hu, M.; Ge, N.; Strachan, J. P.; Li, Z.; Wu, Q.; Barnell, M.; Li, G. L.; Xin, H. L.; Williams, R. S.; Xia, Q.; Yang, J. J. Memristors with Diffusive Dynamics as Synaptic Emulators for Neuromorphic Computing. *Nat. Mater.* **2017**, *16* (1), 101−108.

(27) Yoon, J. H.; Wang, Z.; Kim, K. M.; Wu, H.; Ravichandran, V.; Xia, Q.; Hwang, C. S.; Yang, J. J. An Artificial Nociceptor Based on a Diffusive Memristor. *Nat. Commun.* **2018**, *9* (1), No. 417.

(28) Hasegawa, T.; Terabe, K.; Nakayama, T.; Aono, M. In *Quantum Point Contact Switch Using Solid Electrochemical Reaction*, Extended Abstracts of the 2001 International Conference on Solid State Devices and Materials; SSDM, 2001; pp 7−8.

(29) Hasegawa, T.; Terabe, K.; Tsuruoka, T.; Aono, M. Atomic Switch: Atom/Ion Movement Controlled Devices for beyond von-Neumann Computers. *Adv. Mater.* **2012**, *24* (2), 252−267.

(30) Xu, Z.; Bando, Y.; Wang, W.; Bai, X.; Golberg, D. Real-Time in Situ HRTEM-Resolved Resistance Switching of Ag_2S Nanoscale Ionic Conductor. *ACS Nano* **2010**, *4* (5), 2515−2522.

(31) Hasegawa, T.; Ohno, T.; Terabe, K.; Tsuruoka, T.; Nakayama, T.; Cimzewski, J. K.; Aono, M. Learning Abilities Achieved by a Single Solid-State Atomic Switch. *Adv. Mater.* **2010**, *22* (16), 1831−1834.

(32) Ohno, T.; Hasegawa, T.; Tsuruoka, T.; Terabe, K.; Gimzewski, J. K.; Aono, M. Short-Term Plasticity and Long-Term Potentiation Mimicked in Single Inorganic Synapses. *Nat. Mater.* **2011**, *10* (8), 591−595.

(33) Zhong, Y.; Tang, J.; Li, X.; Gao, B.; Qian, H.; Wu, H. Dynamic Memristor-Based Reservoir Computing for High-Efficiency Temporal Signal Processing. *Nat. Commun.* **2021**, *12* (1), No. 408, DOI: 10.1038/s41467-020-20692-1.

(34) Demis, E. C.; Aguilera, R.; Sillin, H. O.; Scharnhorst, K.; Sandouk, E. J.; Aono, M.; Stieg, A. Z.; Gimzewski, J. K. Atomic Switch Networks - Nanoarchitectonic Design of a Complex System for Natural Computing. *Nanotechnology* **2015**, *26* (20), No. 204003.

(35) Avizienis, A. V.; Sillin, H. O.; Martin-Olmos, C.; Shieh, H. H.; Aono, M.; Stieg, A. Z.; Gimzewski, J. K. Neuromorphic Atomic Switch Networks. *PLoS One* **2012**, *7* (8), No. e42772.

https://doi.org/10.1021/acsaelm.3c01046
ACS Appl. Electron. Mater. 2024, 6, 688−695

(36) Al-Khazali, H. A. H.; Askari, M. R. Geometrical and Graphical Representations Analysis of Lissajous Figures in Rotor Dynamic System. *IOSR J. Comput. Eng.* **2012**, *02* (5), 971−978.
(37) Liang, C.; Terabe, K.; Hasegawa, T.; Aono, M. Resistance Switching of an Individual Ag2S/Ag Nanowire Heterostructure. *Nanotechnology* **2007**, *18* (48), No. 485202.
(38) Scharnhorst, K. S.; Carbajal, J. P.; Aguilera, R. C.; Sandouk, E. J.; Aono, M.; Stieg, A. Z.; Gimzewski, J. K. Atomic Switch Networks as Complex Adaptive Systems. *Jpn. J. Appl. Phys.* **2018**, *57* (3), No. 03ED02.
(39) Du, C.; Cai, F.; Zidan, M. A.; Ma, W.; Lee, S. H.; Lu, W. D. Reservoir Computing Using Dynamic Memristors for Temporal Information Processing. *Nat. Commun.* **2017**, *8* (1), No. 2204.
(40) Kan, S.; Nakajima, K.; Asai, T.; Akai-Kasaya, M. Physical Implementation of Reservoir Computing through Electrochemical Reaction. *Adv. Sci.* **2022**, *9* (6), No. 2104076.
(41) Akai-Kasaya, M.; Takeshima, Y.; Kan, S.; Nakajima, K.; Oya, T.; Asai, T. Performance of Reservoir Computing in a Random Network of Single-Walled Carbon Nanotubes Complexed with Polyoxometalate. *Neuromorphic Comput. Eng.* **2022**, *2* (1), No. 014003.

https://doi.org/10.1021/acsaelm.3c01046
ACS Appl. Electron. Mater. 2024, 6, 688−695